

# A Hybrid Desktop Process for Integrated Deposition and Low-cost, In-situ Sintering of Conductive Silver Nanoparticles

WCMNM  
2017  
No.

Roshan Bhandari, Shalu Bansal, Michael Dexter, Rajiv Malhotra

Department of Mechanical Engineering, Oregon State University

## Abstract

Microscale continuous thin films or patterned conductive structures find applications in thin film electronics, energy generation and functional sensor systems. An emerging alternative to conventional vacuum based deposition of such structures is the additive deposition and sintering of conductive nanoparticles, to enable low temperature, low-cost and low energy fabrication. While significant work has gone into additive deposition of nanoparticles the realization of the above potential needs nanoparticle sintering methods that are equally low-cost, in-situ, ambient condition and desktop-sized in nature. This work demonstrates the integration of non-laser based, low-cost and small footprint optical energy sources for ambient condition sintering of conductive nanoparticles, with wide-area aerosol jet based additive printing of nanoparticle inks. The nanoparticle sintering is characterized by quantifying the sintering temperatures, sintered material conductivity, crystallinity, optical properties, thickness and microscale morphology in terms of the sintering parameters. It is shown that such optical sintering sources can be further integrated with inkjet printing as well, and the implications on new paradigms for hybrid additive-sintering processes for fabrication of functional systems using nanoparticles as building blocks are discussed.

**Keywords:** Nanoparticles, Xenon Light Sintering, Additive Manufacturing

## 1. Introduction and Motivation

Conductive films and patterns are used as conductive backplanes and electrodes in a variety of applications including solar cells, organic light emitting diodes, flexible printed circuits, thin-film transistors, RFID tags, and sensors [1-3]. Conventionally, such films and patterns have been deposited via vacuum based and lithography based processes. More recently, there has been significant interest on replacing such processes with additive deposition and sintering of conductive nanoparticles (NPs) for the above applications. This approach holds the promise of lower sintering temperatures after deposition, due to enhanced surface diffusion and lower melting points of NPs, which can reduce energy consumption and costs. This paradigm has been encouraged further by the maturity of processes for additive deposition of NP inks including inkjet printing [4], aerosol jet printing [5] and micro-extrusion [6]. In addition to the inherent flexibility of these deposition processes, techniques like microextrusion can even be used to deposit NPs on conformal surfaces [6]. Whether the NPs are deposited on planar surfaces for applications like flexible or rigid electronics, or deposited on conformal surfaces for conformal conductive interconnects, a key step after deposition is the sintering of the NPs to enable high conductivity of the deposited structure. Conventional oven-based [7] or microwave-based [8] sintering occurs in a chamber and is not amenable to continuous integration with the above deposition processes. The use of lasers for in-situ NP sintering is limited mainly by the equipment cost, which can significantly exceed the cost of the above additive equipment. Intense Pulsed Light sintering (IPL) uses large-area, visible and broad-spectrum light to sinter the deposited NPs [9, 10]. While IPL operates in the ambient and has significantly greater throughput than

laser sintering, it is comparable to laser sintering in costs. To enable low-cost, desktop and integrated manufacturing of conductive backplanes and electrodes there is a need for a NP sintering process that matches the above additive processes in cost and size, while enabling in-situ and ambient condition sintering.

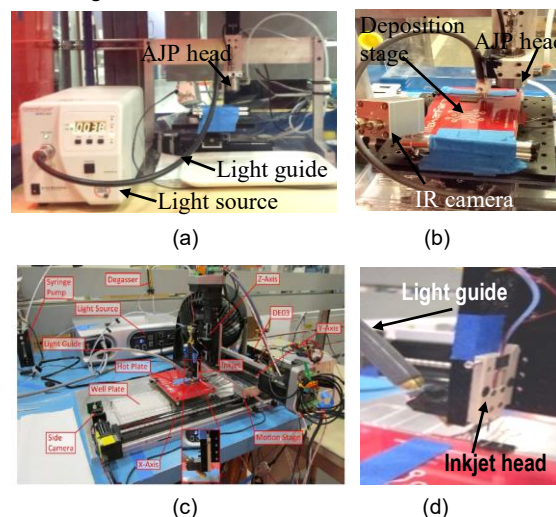


Fig. 1. (a) Integrated xenon-light source and aerosol jet printing (AJP) system (b) Close up of light guide mounted with AJP head (c) Integrated xenon-light source and inkjet printing system (b) Close up of mounted light guide with inkjet printing head.

Our group has been investigating the integration of continuous xenon light sources for NP sintering with additive processes like aerosol jet printing and inkjet printing. These light sources are low-cost (<\$5000), small-footprint (desktop-size), and deliver broad-spectrum visible light (350-800 nm) using light guides to the deposited NPs (Figure 1). This paper

demonstrates one such hybrid process that integrates wide-area aerosol printing (AJP) with the above light sources (Figure 1a-b), for in-situ printing and sintering of Ag conductive NPs, a popular conductive material for the aforementioned applications. The temperature evolution during sintering as well as the conductivity, crystallinity, microstructure and optical properties of the sintered material are characterized in terms of the light guide velocity and number of sintering passes. It is shown that this hybrid process is able to sinter the deposited NPs to conductivities that are usable for the aforementioned applications. Further, we show preliminary results on the integration of inkjet printing with these xenon light sources as a demonstration of the ease of this kind of process hybridization with other NP printing processes. The implications of such hybridization on future efforts in additive manufacturing using NPs are discussed.

## 2. Experimental Methods

Ag NP ink was prepared by suspending Ag NPs (nominal size 20 nm, Sigma Aldrich) in tetradecane at 16% by weight. The NP ink was sonicated for 1 hour to evenly disperse NP in solution after which the NPs stayed in solution for at least 12 hours without dropping out. The inks were deposited at room temperature onto borosilicate glass substrates via the home-made AJP system in Figure 1a-b. This AJP system consists of an ultrasonic AJP head with control system, and a syringe pump, integrated with a 3-axis motion system. The AJP parameters were optimized to obtain the smallest layer thickness possible under room temperature deposition without segregation of the NPs into clumps. The final deposited film thickness used in sintering experiments was nominally 2.6  $\mu\text{m}$  over an area of 20 mm by 1 inch on a borosilicate glass substrate. Note that the thickness of the deposited layer depends on a number of aerosol jet parameters as well as the substrate and the ink composition. Since these phenomena have been well studied [11] and are not the focus of this paper we do not describe this empirical process of selecting AJP process parameters in detail. After deposition, the light from the light guides was used to sinter the deposited NPs within the same setup. The light spot formed a circle of 10 mm diameter on the deposited film and was moved in a rastering path to sinter the entire film (Figure 2a). The overlap  $O$  between consecutive passes was fixed at 80% of the spot diameter. The optical power was fixed at the maximum value, resulting in a total irradiance of 80  $\text{mW}/\text{cm}^2$  at the substrate as measured using an optometer. The temperature evolution along the direction of light guide motion during sintering was measured using a thermal camera (Thermoimager TIM 160) at 5 distinct points (in red in Figure 2a) corresponding to 5 progressive locations of the light guide during sintering. The film thickness was measured using a white light interferometer and was used, along with the sheet resistance measured by a four-point probe, to calculate the bulk electrical resistivity of the sintered film. Scanning Electron Microscopy (SEM, FEI Quanta 3D) and X-ray Diffraction (XRD, Rigaku Ultima-IV) in the Bragg-Brento configuration were used to characterize the degree of sintering in the material. UV-Vis absorption

of the film was measured using a Jasco V670 spectrophotometer with an integrating sphere.

## 3. Results

The measured film temperature is higher when the sintering speed is lower (Figure 2b-d), due to greater residence time of the optical power source over a given region of the film which results in greater total energy absorption. Note that this temperature difference is very little, only around 25°C, for a reduction in speed from 50 mm/min to 15 mm/min. A peculiar effect of the number of passes is seen in Figure 2e-g. After the first pass, the film temperature drops significantly in the second and third passes. The reason for this will be explained along with results on densification. Note that the temperatures shown in Figure 2 are below the melting or surface pre-melting temperatures [12] for Ag NPs used here, indicating the absence of NP melting.

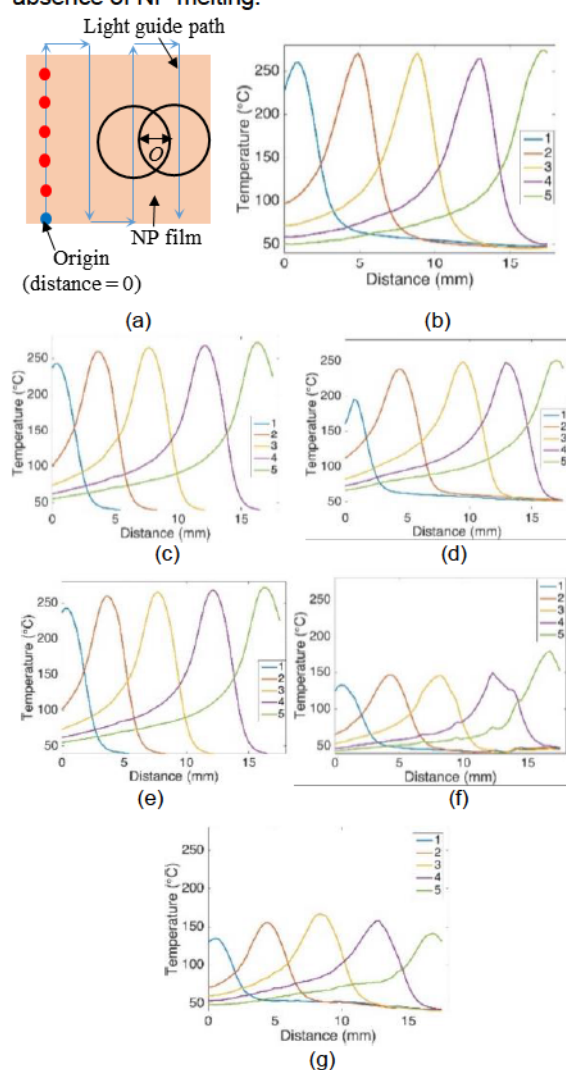


Fig. 2. (a) Guide path and temperature measurement; Temperature for 1 pass at guide speed of (b) 15 mm/min (c) 30 mm/min (d) 50 mm/min; Temperature at guide speed of 30 mm/min for (e) one pass (f) 2 passes (g) 3 passes.

The full width at half maximum (FWHM) from XRD (Figure 3) shows that sintering reduces the FWHM significantly, which indicates increased interparticle necking and particle size due to sintering as per the

Scherrer equation. SEM images (Figure 4a-f) also show evidence of interparticle necking and increase in grain size due to sintering, as well as sintering through the film thickness (Figure 4g-h). Both FWHM and SEM show that greater guide speed reduces densification. However, increasing the number of passes beyond 1 at guide speed of 30 mm/min results in little additional densification.

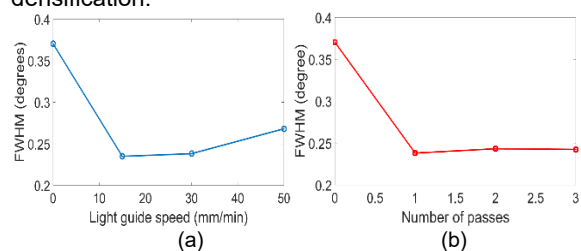


Fig. 3. Change in FWHM as a function of (a) guide speed (b) number of passes. 0 denotes unsintered film.

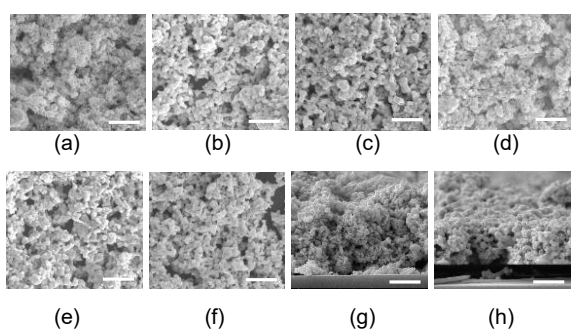


Fig. 4. Planar SEM of (a) unsintered film; films sintered in one pass at (b) 15 mm/min (c) 30 mm/min (d) 50 mm/min; films sintered at 30 mm/min with (e) 2 passes (f) 3 passes. Cross sectional SEM of (g) unsintered film (h) sintered film with one pass at 30 mm/min. All length scales are 1  $\mu\text{m}$ .

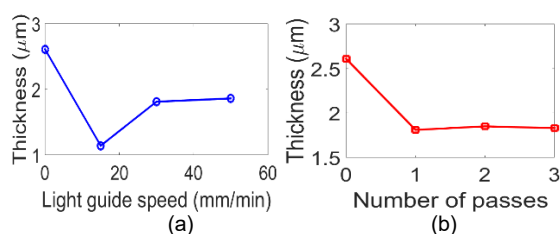


Fig. 5. Change in film thickness as a function of (a) sintering speed (b) number of passes.

While there is a thickness reduction associated with shrinkage during sintering (Figure 5), increase in guide speed shows relatively lesser shrinkage which indicates reduced densification (Figure 5a). Increasing the number of passes from 1 to 3 again shows that the shrinkage and densification is not as high in subsequent passes as it is in pass 1 (Figure 5b). The sheet resistance of the as-deposited films was out of bounds for the four-point probe, and could not be measured, indicating the absence of interparticle necking between NPs in the unsintered film. Tables 1 and 2 show the change in bulk resistivity of the films due to sintering. There is an increase in resistivity with an increase in the guide speed (Table 1), especially at a speed of 50 mm/min, showing a reduction in interparticle necking similar to that seen in Figures 3-5 above. At the same time, the relative reduction in resistivity in passes 2 and 3 is much lesser than that between unsintered film and pass 1 (Table 2), which again shows that densification levels off after pass 1.

The minimum bulk resistivity of the sintered material achieved here (at sintering speed of 15 mm/min in one pass, Table 1) is only 7% higher than that of bulk silver, which is sufficient for most of the aforementioned device applications [9, 13]. This resistivity is similar to that obtained via thermal sintering of silver at 130°C for up to 6 hours (as compared to 20 minutes of sintering time here for the lowest bulk resistivity). This bulk resistivity is also comparable to that obtained by laser sintering (3% higher than bulk silver [13]) and IPL (1.5% higher than bulk silver [13]) while reducing the cost and size of the sintering equipment significantly.

Table 1  
Bulk resistivity as a function of sintering speed

Guide speed for one pass (mm/min)	Bulk Resistivity ( $\mu\Omega\cdot\text{m}$ )
Unsintered	Infinity
15	0.12
30	0.7
50	$1.23 \times 10^5$

Table 2  
Bulk resistivity as a function of number of passes

Number of passes at 30 mm/min guide speed	Bulk Resistivity ( $\mu\Omega\cdot\text{m}$ )
Unsintered	Infinity
1	0.7
2	0.37
3	0.21

The effect of sintering speed on densification can be fairly easily explained. A longer residence time due to slower sintering speed results in slightly higher temperatures but also longer time for which these temperatures are maintained over a given material point on the film. Since mass transfer during interparticle necking increases with higher temperature and longer time over which these temperatures are maintained, slower sintering speeds result in greater densification and lesser resistivity.

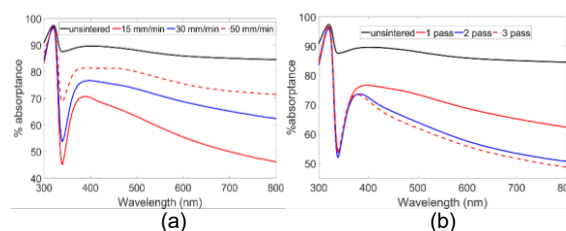


Fig. 6. Change in optical absorption of the film as a function of (a) sintering speed (b) number of passes.

The levelling off in densification with increasing number of passes beyond 1 can be explained based on the fact that NP densification reduces the film's capacity to absorb visible optical energy. This is because of a loss in the nanoscale character of the film, as shown in our previous work [10, 14]. Thus, after densification in pass 1 there is a reduction in the optical energy absorbed in subsequent passes, which reduces the temperature (Figure 2e-g) and the relative increase in densification (Figures 3-5) in passes 2 and 3. This dependence of optical absorption on densification is also observable in the absorbance curves obtained from UV-Vis spectroscopy (Figure 6). There is a large reduction in visible light absorption

from unsintered film to pass 1 (Figure 6b) but a relatively smaller reduction after pass 1. At the same time, the reduction in visible absorption with reducing guide speed can be observed in Figure 6a. Note the Ag film used here was thick enough that transmittance was zero. The change in absorption was calculated via the change in reflectance, as measured by the integrating sphere in the spectrophotometer. This xenon lamp light source was also integrated with a piezo-electric inkjet head on a 3-axis gantry system (Figure 1c-d) to print and in-situ sinter silver lines on Kapton substrates within the same process setup. Representative optical image of such lines are shown in Figure 7a. XRD plots (Figure 7b) and SEM images (Figure 7c-f) show that NP densification in printed patterns can be achieved by this approach. Further, there is minimal distortion of the substrate during sintering. Note that this integration was performed via nothing more than a change in the fixture used to mount the light guide.

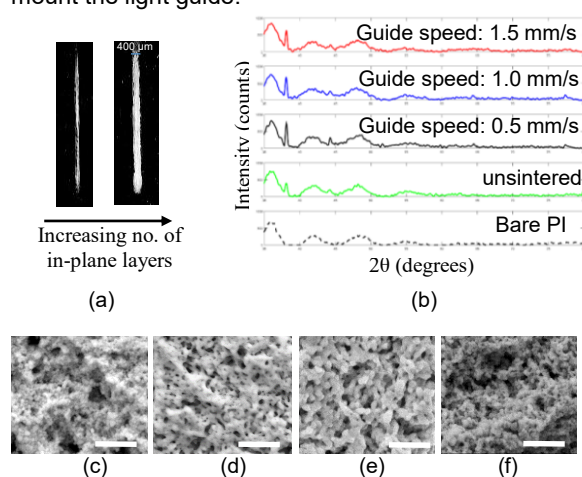


Fig. 7. (a) optical images of printed and sintered lines (b) Change in XRD peak intensities with a change in guide speed during sintering; SEM images of (c) unsintered lines and sintered lines at guide speeds of (d) 0.5 mm/s (e) 1.0 mm/s (f) 1.5 mm/s

#### 4. Conclusions

This paper demonstrates the facile integration of a low-cost, desktop scale xenon lamp light source with NP deposition methods like aerosol jet for in-situ deposition and sintering of conductive NPs. The sintered material conductivity achieved is usable for flexible and rigid electronics while the equipment cost and size is much lesser than laser-based or conventional intense pulsed light sintering. The characterization of temperature evolution, densification and conductivity shows that while slower sintering speed increases conductivity, increasing the number of passes has relatively lesser impact on increasing densification. This is because once densification begins and the nanoscale features in the film are reduced there is a reduction in optical absorption, subsequent temperature rise and in further densification. We also show that such low-cost, desktop xenon lamp sources can easily be integrated with deposition techniques beyond aerosol-jet, e.g., the inkjet printing setup in Figure 1c-d, without any additional equipment or costs. A particularly attractive quality of this hybrid process is that additive manufacturing with NPs can be enabled without the

need for sintering within a chamber (e.g., oven based sintering) which causes discontinuity in the process, and without the costs of a laser for sintering. It is interesting to note that xenon lamps with a similar power spectrum but with a greater irradiance have been used to sinter other metallic and non-metallic NPs as well. Thus, there is potential to use the kind of hybrid process discussed here for fabrication of functional devices, beyond conductive interconnects, as well. Our future work will attempt to realize this potential by adding on further xenon lamps to increase the incident power density

#### Acknowledgements

The authors acknowledge the support provided from National Science Foundation grant #1537196.

#### References

- [1] M. Allen et al., "R2R gravure and inkjet printed RF resonant tag". *Micro. Engg.*, 2011. 88(11): 3293-3299.
- [2] G. Iannaccone et al., "Roll-to-roll compatible flexible polymer solar cells incorporating a water-based solution-processable silver back electrode with low annealing temperature". *Sol. En. Mats.*, 2015. 143: 227-235.
- [3] M. Vilkmann et al., "Fully roll-to-roll processed organic top gate transistors using a printable etchant for bottom electrode patterning". *Org. Elecs*, 2015. 20: 8-14.
- [4] F.C. Krebs, "Fabrication and processing of polymer solar cells: A review of printing and coating techniques". *Sol. En. Mats.*, 2009. 93(4): 394-412.
- [5] M. Ha et al., "Aerosol Jet Printed, Low Voltage, Electrolyte Gated Carbon Nanotube Ring Oscillators with Sub-5  $\mu$ s Stage Delays". *Nan. Lets.*, 2013. 13(3): 954-960.
- [6] J.E. Smay et al., "Ceramics and Composites Processing Methods", 2012, Wiley & Sons: 459-484.
- [7] J.J. Adams et al., "Conformal Printing of Electrically Small Antennas on Three-Dimensional Surfaces". *Adv. Mats.*, 2011. 23(11): 1335-1340.
- [8] J. Perelaer et al., "Plasma and Microwave Flash Sintering of a Tailored Silver Nanoparticle Ink, Yielding 60% Bulk Conductivity on Cost-Effective Polymer Foils". *Adv. Mats.*, 2012. 24(29): 3993-3998.
- [9] Y. Galagan et al., "Photonic sintering of inkjet printed current collecting grids for organic solar cell applications". *Org. Elecs*, 2013. 14(1): 38-46.
- [10] S. Bansal et al., "Nanoscale-shape-mediated coupling between temperature and densification in intense pulsed light sintering". *Nano.*, 2016. 27(49): 495602-16.
- [11] A. Mahajan et al., "Optimization of Aerosol Jet Printing for High-Resolution, High-Aspect Ratio Silver Lines". *ACS App. Mats. & Int.*, 2013. 5(11): 4856-4864.
- [12] H.A. Alarifi et al., "Determination of complete melting and surface premelting points of silver nanoparticles by molecular dynamics simulation". *The Phys. Chem. C*, 2013. 117(23): 12289-12298.
- [13] J. Niittynen et al., "Alternative sintering methods compared to conventional thermal sintering for inkjet printed silver nanoparticle ink". *Thin Solid Films*, 2014. 556(0): 452-459.
- [14] W. MacNeill et al., "On the self-damping nature of densification in photonic sintering of nanoparticles". *Scientific Reports*, 2015. 5: 14845-13.